Experimental and Molecular Pathology 94 (2013) 386–397

Contents lists available at SciVerse ScienceDirect

Experimental and Molecular Pathology

journal homepage: www.elsevier.com/locate/yexmp

Cytomegalovirus-induced salivary gland pathology: AREG, FGF8, TNF-α, and IL-6 signal dysregulation and neoplasia

Michael Melnick [a,*], Krysta A. Deluca [a], Parish P. Sedghizadeh [b], Tina Jaskoll [a]

[a] Laboratory for Developmental Genetics, USC, USA
[b] Oral and Maxillofacial Pathology, Division of Diagnostic Sciences, USC, 925 W 34th Street, Los Angeles, CA, 90089-0641 USA

ARTICLE INFO

Article history:
Received 8 November 2012
and in revised form 10 January 2013
Available online 8 February 2013

Keywords:
Cytomegalovirus
CMV-induced pathology
Salivary gland
AREG
FGF8
IL-6
TNF-α

ABSTRACT

Mucoepidermoid carcinoma (MEC) is the most common malignant tumor originating in major and minor salivary glands (SGs). Although the precise multifactorial etiology of human SG-MEC is largely unknown, we have recently shown that cytomegalovirus (CMV) is an important component of MEC tumorigenesis. Despite the well-documented overexpression of the EGFR→ERK signaling pathway in SG-MEC, there has been limited to no clinical success with inhibition of this pathway. Using our previously characterized mouse model of CMV-induced SG dysplasia/neoplasia, we report that inhibitors of the EGFR→ERK pathway do not ameliorate or rescue well-established pathology, either singly or in combination, but they do inhibit the evolution of progressive pathogenesis ("disease tolerance") in the face of mounting CMV burden. Failure to rescue SG pathology, suggested a possible increase in the ligand levels of alternative pathways that share cell proliferation and survival effectors (e.g. ERK and PI3K). Here we present evidence of a highly significant upregulation of ligands for the EGFR, FGFR, IL-6R, and TNFR signaling pathways, all of which converge upon the Raf/MEK/ERK amplifier module. This explains our finding that even in the presence of the highest nontoxic dose of an ERK phosphorylation inhibitor, pERK is undiminished. Given the considerable pathway crosstalk, a deep understanding of subversion and dysregulation of the SG interactome by CMV is a priori quite daunting. Circumventing this dilemma, we present evidence that concurrent inhibition of ERK phosphorylation (U0126) and CMV replication (acyclovir) obviates progressive pathogenesis and results in complete SG rescue (tumor regression). These findings provide a mechanistic foundation for potential clinical trials that utilize similar concurrent treatment with extant FDA-approved drugs.

Introduction

Human cytomegalovirus (hCMV) is common, 50–90% of adults being seropositive, depending on geographical location and socioeconomic status (Boppana and Fowler, 2007). Like other DNA herpes viruses, hCMV establishes lifelong persistence and latent infection following primary exposure; the precise triggering mechanisms that promote hCMV reactivation in immunocompetent persons are unknown (Yuan et al., 2009). Of special interest, hCMV, both active and latent, has a particular tropism for salivary glands (Nichols and Boeckh, 2000; Wagner et al., 1996).

We have recently confirmed that hCMV is a principle element in the multifactorial causation of salivary gland (SG) mucoepidermoid carcinoma (MEC) (Melnick et al., 2012). Active hCMV protein expression positively correlates with over 90% of SG-MEC tumor cases; active hCMV also correlates and colocalizes with upregulation and activation of an established oncogenic signaling pathway (COX/AREG/EGFR/ERK).

That human SG-MEC is a virally implicated pathology, is further supported by our finding that purified mouse CMV (mCMV) induces cellular pathology in an in vitro mouse SG organ model that displays a number of histologic and molecular characteristics similar to human MEC (Jaskoll et al., 2011; Melnick et al., 2011). Specifically, we have demonstrated that mCMV induces (1) mesenchymal-to-epithelial transformation (MET); (2) epithelial and mesenchymal hyperplasia, dysplasia and neoplasia; (3) loss of basement membrane zone components, reduced expression of epithelial-specific adherens junction proteins (E-cadherin, p120), and admixing of stromal-derived and epithelial-derived cells; (4) expression of CRTC1 protein, a protein found in SG MECs but not in normal SG tissue (Tirado et al, 2007); and (5) upregulation of the activated COX/AREG/EGFR/ERK signaling pathway. Further, the neoplastic phenotype is initially ameliorated by treatment with small molecule inhibitors of several key targets in the autocrine loop; inhibition of ERK phosphorylation completely precluded pathology, but less so with inhibitors of COX or EGFR. This suggested that other receptor tyrosine kinases mediating signals

* Corresponding author at: Laboratory for Developmental Genetics, University of Southern California, 925 W 34th Street, DEN 4266, MC-0641, Los Angeles, CA 90089-0641, USA. Fax: +1 213 740 7560.
E-mail addresses: mmelnick@usc.edu (M. Melnick), kad_189@usc.edu (K.A. Deluca), sedghiza@usc.edu (P.P. Sedghizadeh), tjaskoll@usc.edu (T. Jaskoll).

0014-4800/$ – see front matter © 2013 Elsevier Inc. All rights reserved.
http://dx.doi.org/10.1016/j.yexmp.2013.01.005

that converge downstream on ERK are also likely to play a key role in SG tumorigenesis (e.g. FGFR).

Since CMV and other viruses commonly hijack host cell molecular networks for self-propagation, eliciting concomitant cellular pathology, obvious questions remain. Among these are: Given the widespread resistance to anticancer kinase inhibitors (Engelman and Settleman, 2008; Wilson et al., 2012), can inhibitors of EGFR and ERK phosphorylation ameliorate or rescue well-established mouse SG pathology? Given that virally implicated pathology is routinely associated with perturbations to multiple host signaling pathways (Gulbahce et al., 2012; Rozenblatt-Rosen et al., 2012), what additional pathways might be dysregulated by mouse CMV proteins?

To address these questions, we have designed a series of mechanistic experiments and report that inhibitors of the EGFR→ERK pathway do not ameliorate or rescue well-established pathology, either singly or in combination, but they do inhibit the evolution of progressive pathogenesis, a sort of "disease tolerance" in the face of mounting CMV burden (Medzhitov et al., 2012). Further, complete rescue with an antiviral nucleoside analogue, acyclovir, in combination with a kinase inhibitor, indicates that mCMV replication is necessary to maintain SG pathogenesis. In this regard, mCMV-associated kinase inhibitor resistance appears to be related to increased expression and activation of the targeted kinase (ERK), along with the dysregulation of alternative signaling pathways that promote downstream cell proliferation and survival. Transcriptional analysis identified several of these dysregulated host cell pathways in addition to EGFR→ERK: FGF8, IL-6, TNF-α. All four growth factors and cytokines are primarily localized to the abnormally abundant stroma and its resident dysplastic/neoplastic fibroblasts. Targeting this enabling microenvironment may have therapeutic importance.

Materials and methods

Animals

Timed pregnant inbred C57/BL6 female mice (Charles River, Wilmington, MA) were purchased from Charles River (Wilmington, MA) (plug day = day 0 of gestation) and newborn (NB) mice were harvested as previously described (Melnick et al., 2006, 2009). All protocols involving mice were approved by the Institutional Animal Care and Use Committee (USC, Los Angeles, CA).

Organ culture

Newborn (NB) submandibular glands (SMGs) were dissected and cultured for 6 (NB + 6) or 12 days (NB + 12) using a 3D organ culture system and BGJb medium (Invitrogen Corporation, Carlsbad, CA) as previously described (Melnick et al., 2006). This SMG organ culture system maintains the three-dimensional architecture and microenvironment associations between epithelial and stromal cells seen in vivo. Briefly, SMG organs were cultured on small discs of Nucleopore filter (150 μm thick, with 0.8 μm pores) placed upon a stainless steel supporting grid (~15–25 filters per grid). The grids were then placed on the inner ring of Grobstein culture dishes and 1 ml of medium was added to the well below the grid. The SMG organs develop at the air/medium interface, with the 1×10^5 plaque-forming units (PFU)/ml of *lac*Z-tagged mCMV RM427+ (Saederup et al., 1999) in BGJb medium being below the grid on day 0 for 24 h and then with virus-free medium for the remaining culture period; controls consisted of SMGs cultured in control medium for the entire period. Media was changed daily. 3D SMG organs were not "bathed in" mCMV-infected medium as in cell and tissue culture systems, exposed to virus-infected medium for the entire culture period, nor inoculated with virus. SMGs were collected and processed for hematoxylin and eosin histology, immunolocalization or Western blot analysis. For histology, and immmunolocalization analysis, SMGs were fixed for 4 h at 4 °C in Carnoy's fixative or 10% neutral buffered formalin, embedded in low melting point paraplast, serially-sectioned at 8 μm and stained as previously described (Melnick et al., 2006).

Assay of mCMV infection: we assayed for β-galactosidase (*lacZ*) activity essentially as previously described (Melnick et al., 2006). β-Galactosidase-stained whole mounts were then dehydrated through graded alcohols, embedded in paraffin, serially-sectioned and counterstained with eosin. β-Galactosidase-stained plaques appear blue and unstained tissue appears pink.

Immunolocalization

Cultured SMGs were serially-sectioned at 8 μm and immunostained as previously described (Melnick et al., 2006, 2009) using the following commercially-available polyclonal antibodies: pERK1/2 (Thr202/Tyr204); Amphiregulin; and IL-6 (M-19) (Santa Cruz Biotechnology, Inc, Santa Cruz, CA); FGF8 and TNFα (Abcam, Cambridge, MA). Nuclei were counterstained with 4′,6-Diamidino-2-phenylindole, dihydrochloride (DAPI) (Invitrogen Corporation). Negative controls were performed in parallel under identical conditions and consisted of sections incubated without primary antibodies. For each treatment group, 3–6 SMGs per day were analyzed. All images were acquired with a Zeiss Axioplan microscope equipped with a SPOT RT3 camera and processed with SPOT Advanced and Adobe Photoshop CS2 software.

Western blot analysis

Newborn (NB) SMGs cultured for 6 (NB + 6) or 12 (NB + 12) uninfected (control) and mCMV-infected SMG organs were collected; each independent sample consisted of 3–4 SMGs per group. Proteins (25–35 μg) were separated by SDS-PAGE gels, transferred to a PVDF membrane, stained with antibodies overnight and the membranes were subjected to chemiluminescence detection (ECL) according to the manufacturer's instructions (ThermoScientific, Rockford, IL) as previously described (Melnick et al., 2006) Antibodies: pERK1/2 (Thr202/Tyr204) and β-actin (Santa Cruz Biotechnology). Data was quantitated using the ImageJ image analysis software (NIH) and normalized to the level of β-actin expression in each sample.

Statistical analysis

Significant differences between mCMV-infected and control SMGs, as well as between mCMV and mCMV + treatment SMGs, were determined by student t-test, with $\alpha = 0.05$ and the null hypothesis of $R = 1$. The calculated expression ratios (Rs) were log or arcsin transformed prior to analysis.

Interruption studies

(1) Targeting of EGFR→ERK signaling: To interrupt EGFR signaling, we employed 10 μM gefitinib (GEF) (Selleck Chemicals LLC, Houston, TX), a small molecule inhibitor which blocks the binding of ATP to the intracellular TK domain of EGFR to inhibit EGFR signaling, as described previously (Melnick et al., 2011). To interrupt ERK signaling, we employed 10 μM U0126 (EMD Chemicals, Inc, Gibbstown, NJ), a potent and specific inhibitor of MEK-mediated ERK1 and ERK2 phosphorylation, as previously described (Melnick et al., 2011). These concentrations were previously shown to be the optimal, nontoxic dose that substantially precludes mCMV-induced pathology on day 6 of culture (Melnick et al., 2011). NB SMG organs were infected with 1×10^5 PFU/ml mCMV for 24 h and in control medium until day 6. Beginning on day 6 (NB + 6), mCMV-infected SMG organs were cultured in the presence or absence of either 10 μM GEF or 10 μM U0126 in control medium for an additional 8 days, a total of 14 days in culture (NB + 14). (2) Co-targeted inhibition of

the EGF→ERK pathway: NB SMG organs were infected with 1×10^5 PFU/ml mCMV for 24 h and cultured control medium until day 6. Beginning on day 6, explants were cultured in the presence or absence of 10 μM GEF + 10 μM U1026 (D6GEF + D6U) for an additional 8 days, a total of 14 days in culture (NB + 14). (3) Inhibition of CMV replication: To inhibit CMV replication, we used 10 μg/ml acyclovir sodium (American Pharmaceutical Partners, Inc, Schaumberg, Il), a synthetic purine nucleoside analogue which is a highly selective agent for CMV with low toxicity to the host cell (Burns et al., 1981) and previously shown to inhibit mCMV infection in mouse SMGs in vitro (Melnick et al., 2006); this concentration was previously shown to be the optimal, nontoxic dose (Melnick et al., 2006). NB SMG organs were infected with 1×10^5 PFU/ml mCMV for 24 h and cultured in control medium until day 6. Beginning on day 6, mCMV-infected SMGs were cultured in the presence 10 μg/ml acyclovir, 10 μM U0126 + 10 μg/ml acyclovir, 10 μM GEF + 10 μg/ml acyclovir or no drugs for an additional 8 days, a total of 14 days in culture (NB + 14). Controls consisted of uninfected SMGs without treatment or with D6GEF, D6U0126, or D6Acy treatment (singly or in combination) cultured for 14 days. No differences were seen between untreated and inhibitor-treated uninfected SMGs; untreated controls are presented. In all experiments, media was changed daily and treatments (GEF, GEF + U0126, or U0126 with/without acyclovir) were added daily beginning on day 6.

Quantitative RT-PCR

For analysis of gene expression, qRT-PCR was conducted as previously described (Melnick et al., 2006, 2009) on NB + 6 control and mCMV-infected samples; each sample consisted of 4–5 pooled explants. RNA was extracted and 1μg RNA was reverse transcribed into first strand cDNA using ReactionReady™ First Strand cDNA Synthesis Kit: C-01 for reverse transcription (SABiosciences, Frederick, MD). The primer sets used were prevalidated to give single amplicons and purchased from SABiosciences (Frederick, MD): Areg (PPM02976A); Egf (PPM03703A); Fgf8 (PM02962A); Il6 (PPM03015A); Tnfa (PPM03113A). Primers were used at concentration of 0.4 μM. The cycling parameters were 95 °C, 15 min; 40 cycles of (95 °C, 15 s; 55 °C, 30–40 s and 72 °C, 30 s). Specificity of the reactions was determined by subsequent melting curve analysis. RT-PCRs of RNA (not reverse transcribed) were used as negative controls. GAPDH was used to control for equal cDNA inputs and the levels of PCR product were expressed as a function of GAPDH. The relative fold changes of gene expression between the gene of interest and GAPDH, or between the NB + 6 control and mCMV-infected samples, were calculated by the $2^{-\Delta\Delta CT}$ method. Significant expression differences between mCMV-infected and control samples were determined by student t-test, with $\alpha = 0.01$ and the null hypothesis of $R = 1$, where R is the mean relative expression ration (mCMV/control) across the entire sample. Expression ratios were log transformed prior to analysis to satisfy the assumption of normality.

Probabilistic neural network (PNN) analysis

We used PNN analyses to determine the contribution of each individual gene to the discrimination between experimental groups with 100% sensitivity and specificity (Melnick et al., 20011). As such, PNN analyses identify the relative importance (0–1, with 0 being of no relative importance and 1 being relatively most important) of specific gene expression changes that discriminate between phenotypes. It is the contextual change in expression, not the direction of change, which is important in defining the molecular phenotype. The foundational algorithm we used is based upon the work of Specht and colleagues (Chen, 1996; Specht, 1988; Specht and Shapiro, 1991). The proprietary software designed by Ward Systems Group (Frederick, MD) formulates Specht's procedure around a genetic algorithm (Goldberg, 1989).

Results

The trajectory of this research is to identify molecular targets that may prove critical to a therapeutic solution. To this end, one has always to discern patterns of covarying molecular and histopathologic phenotypes, relating measurements and localization of transcripts and proteins (input) to a well-characterized pathologic phenotype (output). Here we utilize an in vitro 3D submandibular gland (SMG) organ culture strategy previously shown to induce cellular pathology resembling secretory gland neoplasia (Jaskoll et al., 2011; Melnick et al., 2006, 2011).

Progressive histopathology

Newborn (NB) mouse SMGs are cultured in 1×10^5 PFU/ml mCMV for 24 h and maintained in control medium for a total of 6 or 12 days; controls consist of NB SMGs cultured for identical periods in control medium. Our novel 3D SMG organ culture system maintains the morphological integrity, 3D architecture and microenvironment seen in in vivo SMGs. As we have previously reported (Melnick et al., 2011) and replicate here (Fig. 1), mCMV infection induces a severe cytopathic effect (CPE), one which becomes progressively more severe in the period from 6 to 12 days in culture. Control SMGs on days 6 and 12 are characterized by densely packed, branched, cuboidal epithelia; these acini and ducts are embedded in a sparse fibromyxoid stroma containing variable numbers of stellate to ovoid fibroblasts (Figs. 1A, C). mCMV-infected SMGs cultured for 6 days (NB + 6) are characterized by a marked diminution of branching epithelia, acini and ducts; abnormal duct epithelia is hypoplastic and pseudo-stratified and the lumina are dilated and filled with cellular debris (Fig. 1B). These dysplastic epithelial components are embedded in a substantial, hypercellular stroma primarily composed of giant basophilic round cells mixed with far fewer and smaller eosinophilic cells (Fig. 1B).

mCMV-infected SMGs cultured for 12 days (NB + 12) exhibit a more severe viral CPE in the stroma, and abnormal parenchyma consistent with a tumorigenic phenotype (Fig. 1D). The marked increased stromal cellularity is composed of sheets of large basophilic, pleomorphic cells and smaller eosinophilic cells with high nuclear-to-cytoplasm ratios, prominent nuclei and nucleoli, and frequent kidney-shaped nuclei pathognomonic of CMV infection (Alwine, 2012). The increasingly sparse branched epithelia frequently display severely dilated lumina, and individual cells with increased nuclear-to-cytoplasmic ratios, hyperchromatism, and visible nucleoli. Intraluminal and extrabasal proliferation of epithelial cells is often seen, imparting a multilayered appearance to these epithelial islands. Further, a spectrum of

Fig. 1. mCMV induced notable changes in morphology and pERK protein expression in NB + 6 and NB + 12 SMGs. A–D Histological analyses. Control SMGs (A, C) are characterized by densely packed, branched cuboidal epithelial ducts and pro-acini (e) surrounded by fibromyxoid stroma (black *) consisting of stellate to ovoid fibroblasts. mCMV-infected SMGs (B, D) show significant viral CPE in the stroma and epithelial dysplasia consisting of a decrease in branched epithelia, severely dilated lumina (red *), and multi-layered cuboidal epithelia (double black arrows). These abnormal epithelial structures are embedded in a hypercellular stroma (black *) composed of large basophilic, pleiomorphic cells and smaller eosinophilic cells. E-H. mCMV induced pERK protein expression in NB + 6 and NB + 12 SMGs. E–J. Comparison of cell specific immunolocalization of pERK in NB + 6 and NB + 12 control (E, G) and mCMV-infected (F, H) SMGs. In control SMGs (E, G), little immunodetectable pERK is seen. In contrast, mCMV-induced a notable increase in immunodetectable pERK primarily in abnormal stroma (compare F to E and H to G). I–J. Western blot analysis of pERK expression in NB + 6 (I) and NB + 12 (J) control and mCMV-infected SMGs. Comparisons of levels of pERK proteins show a significant increase with mCMV infection on both days 6 and 12 of culture. Bar: 50 μm.

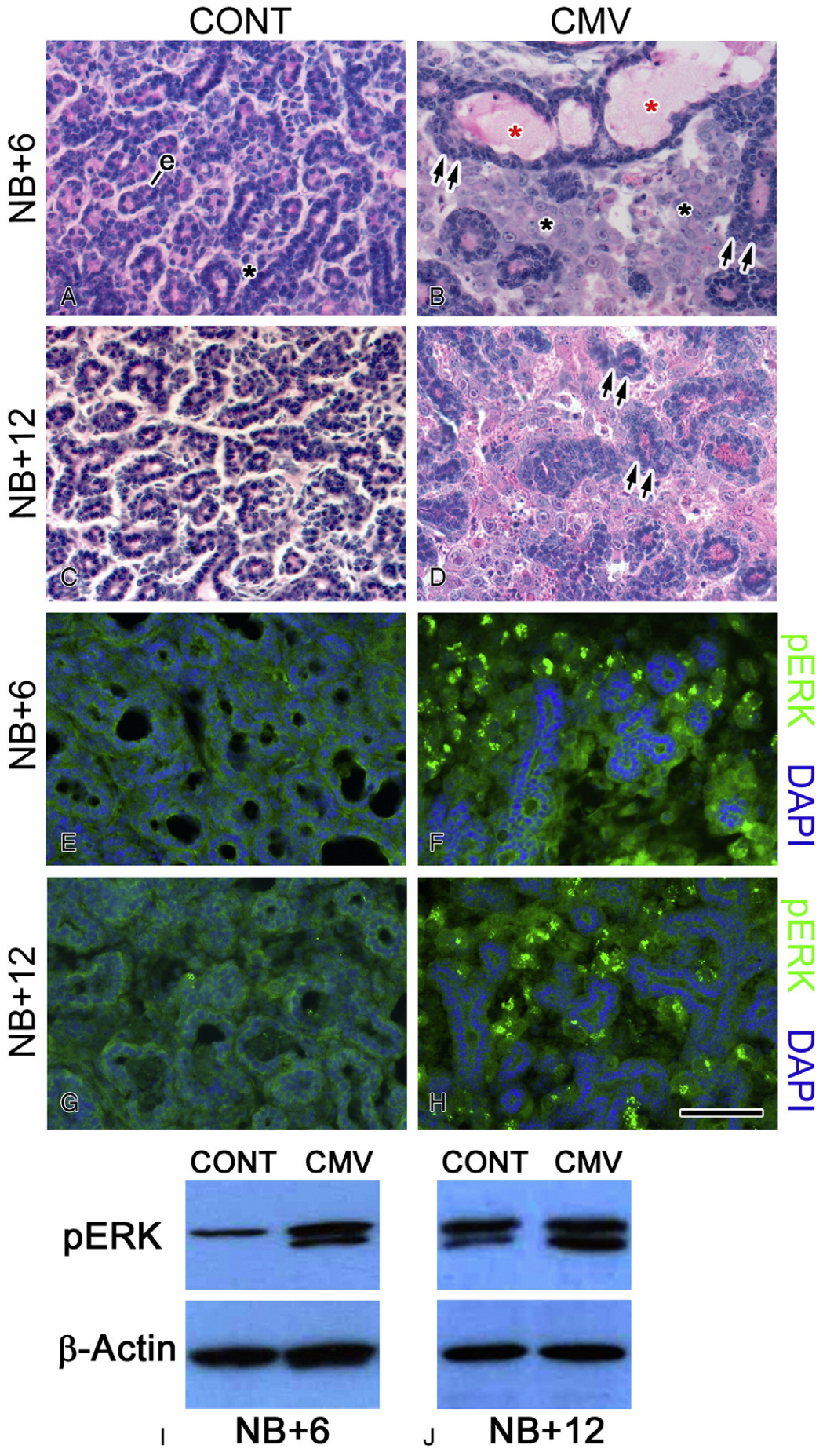
CONT
CMV
NB+6
NB+12
e
A
B
C
D
E
F
G
H
pERK
DAPI
pERK
DAPI
CONT CMV
CONT CMV
pERK
β-Actin
I NB+6
J NB+12

morphotypes, from dysplastic to *in situ* to invasive, can be seen in the abnormal epithelia. Finally, pyknotic, karyorhexic and karyolitic debris is often seen in the lumina of epithelial islands.

pERK expression, viral distribution and inhibition

Previously we reported that upregulation of ERK phosphorylation (pERK) is necessary for initial mCMV-induced pathogenesis (Melnick et al., 2011). Here we confirm that mCMV infection induces a notable increase in pERK expression in NB + 6 and NB + 12 SMGs compared to uninfected controls (Fig. 1; compare F to E and H to G). pERK is immunolocalized almost entirely to cytomegalic stromal cells and is difficult to detect in controls. With mCMV infection, Western blot analysis reveals a significant 40% increase in NB + 6 SMGs ($p<0.05$) and a significant 50% increase in NB + 12 SMGs ($p<0.01$) as compared to uninfected controls (Figs. 1I, J). This increase is not significantly greater on day 12 than on day 6 ($p>0.50$).

The importance of upregulated EGFR→ERK signaling to CMV-induced SG tumorigenesis has been demonstrated in humans and mice (Melnick et al., 2011, 2012). Thus, the EGF→ERK pathway would seem the most parsimonious first target for drug-mediated SG tumor regression. To date, however, EGFR inhibitors have proven largely ineffective for human SG tumors (Bell and Hanna, 2012; Gillespie et al., 2012).

The input signal coming from activated EGFR proceeds through activated SOS and Ras. As a functional unit, the ERK pathway resembles a negative feedback amplifier (NFA) with an amplifier consisting of a three-tiered kinase module Raf-MEK-ERK and feedbacks emanating from ERK to SOS and Raf activation; the ratio of protein abundances of Raf, MEK and ERK is about 1:3:6 (Sturm et al., 2010). The remarkable design principles of the NFA recapitulates that they were often used in electronic circuits to confer robustness, output stabilization, and linearization of nonlinear signal amplification (Sturm et al., 2010). As expected, these properties are determinative of activation kinetics and drug (small molecule inhibitor) response, positive and negative. Here in NB + 6 SMGs with well-established mCMV-induced pathology, we utilized an EGFR inhibitor (gefitinib/GEF) or an inhibitor of MEK-mediated, ERK phosphorylation (U0126) to attempt to rescue the abnormal gland.

NB SMG organs were infected with 1×10^5 PFU/ml mCMV for 24 h and then cultured in control medium to day 6; beginning on day 6, NB SMG organs were then cultured in control medium with or without 10 μM GEF or 10 μM U0126 for an additional 8 days, a total of 14 days in culture (NB + 14). mCMV-infected SMGs treated with GEF beginning on day 6 had some phenotypic improvement compared to untreated, mCMV-infected NB + 14 SMGs, with there being continued evidence of epithelial and stromal pathology (compare Fig. 2D to A). pERK immunostaining was similar in GEF-treated and untreated mCMV-infected NB + 14 SMGs (compare Fig. 2E to B); there is a slight reduction in β-galactosidase-stained virus distribution (compare Fig. 2F to C). NB + 14 mCMV-infected SMGs treated with U0126 beginning on day 6, in contrast to GEF-treated, were most improved from the NB + 6 starting pathology (compare Fig. 2G to 1B); exhibiting less pERK immunostaining than either untreated or GEF-treated mCMV-infected NB + 14 SMGs (compare Fig. 2H to B, E), as well as a slight reduction in β-galactosidase-stained virus. Still, they are characterized by decreased branched acini and ductal epithelia with dilated lumina, as well as hypercellular, cytomegalic stroma. The apparent mitigation of pathology with GEF or U0126 treatment occurs in the presence of considerable mCMV burden (Figs. 2F, I), suggesting that these inhibitors are decreasing host susceptibility to tissue damage (i.e. increasing tolerance to pathology burden).

To secure more complete and longer-term sensitivity to ERK pathway inhibition, modeling and cell culture studies suggest concurrent inhibition of targets inside and outside the NFA (Little et al., 2011; Sturm et al., 2010). For this study, mCMV-infected NB + 6 SMGs were cultured in control medium with or without 10 μM GEF + 10 μM U0126 for an additional 8 days, for a total of 14 days in culture (NB + 14). Other than the near absence of ductal dilation, the histopathology was similar to SMGs treated beginning on day 6 with U0126 alone (compare Fig. 3J to G), and the pERK expression and mCMV burden are comparable (compare Fig. 2K to H and L to I).

Finally, regardless of treatment (GEF, U0126, GEF + U0126), pERK imunolocalization in NB + 14 SMGs is only marginally different from one another, and from untreated mCMV-infected NB + 14 SMGs (Figs. 2B, E, H, K), i.e. pERK expression is marked and the protein is immunolocalized primarily to an abnormal stroma with high mCMV burden (Figs. 2C, F, I, L). This strongly suggests that other mediators whose signals converge downstream on the ERK pathway are at play.

Dysregulation of ligands associated with multifunctional pathways

Wilson et al. (2012) report that an increase in the ligand levels of alternative pathways that share cell proliferation and survival effectors (ERK and PI3K) confers resistance to inhibitors of an "oncogenic" kinase with a similar signaling output. In selecting other multifunctional pathways to investigate, we were cognizant that the parallels between organogenesis and tumorigenesis are ever more apparent (e.g. Becker et al., 2012). Functional studies in our laboratory and elsewhere have demonstrated that SMG organogenesis is regulated through interconnected growth factor and cytokine mediated multifunctional signaling pathways, many of which converge downstream on ERK and PI3K (Jaskoll and Melnick, 1999; Jaskoll et al., 2002, 2004; Kashimata et al., 2000; Melnick and Jaskoll, 2000; Melnick et al., 2001a,b,c). The hub of this complex network of parallel and broadly related pathways is NFκB (Melnick et al., 2001b).

In the present studies, we employed real-time quantitative PCR (qRT-PCR) to determine mCMV-induced transcriptional changes in a group of ligands mediating cognate ERK signaling pathways (EGFR, FGFR, IL-6R, TNGR) (Fig. 3). We performed qRT-PCR on NB + 6 control ($n=6$) and mCMV-infected ($n=6$) SMG samples; each sample consisted of 3–4 pooled explants. Both groups were compared to the starting explants (NB + 0), and these relative expression ratios (R) were compared to each other (Table 1). R is the mean increase or decrease in gland gene expression in NB + 6 uninfected or mCMV-infected glands compared to the starting glands (NB + 0). The variation of R is calculated as gene expression noise (η); the value of η (0 to 1) reflects fluctuations in levels of promotor-binding, transcription factor abundance, post-transcriptional modifications, etc. (Raser and O'Shea, 2005). Of the 6 ERK pathway ligand genes measured, 5 exhibited statistically significant expression differences between untreated and mCMV-infected NB + 6 SMG explants. mCMV infection had no effect on *Egf* expression, downregulated *Tgf-a* expression, and upregulated *Areg* (4-fold), *Fgf8* (5-fold), *Il-6* (64-fold), and *Tnf-α* (2-fold) expression. All four upregulated cognate proteins are immunolocalized primarily to the abnormally abundant, hypercellular stroma of mCMV-infected SMGs (Figs. 4B, D, F, H). These finding are expositive of those seen with attempted inhibition of MEK-mediated, ERK phosphorylation (Fig. 2).

Finally, we utilized probabilistic neural network (PNN) analyses to identify the relative importance (0–1, with 0 being of no relative importance and 1 being relatively most important) of specific gene expression changes to the mCMV-induced pathologic SMG phenotype. Our unbiased optimization algorithm reveals that with the transcript level of just these 4 genes (*Areg*, *Fgf8*, *Il-6*, *Tnf-α*) NB + 6 SMGs can be classified as mCMV-infected or not with 100% sensitivity and 100% specificity (no false negatives; no false positives) (Fig. 4I). Interestingly, *Fgf8* and *Il-6* transcript levels are relatively much more important than *Areg* and *Tnf-α* in the unbiased classification of pathology.

mCMV replication and progressive pathogenesis

We previously found that completion of the viral replication cycle beyond DNA replication is critical to the initiation of SMG pathogenesis

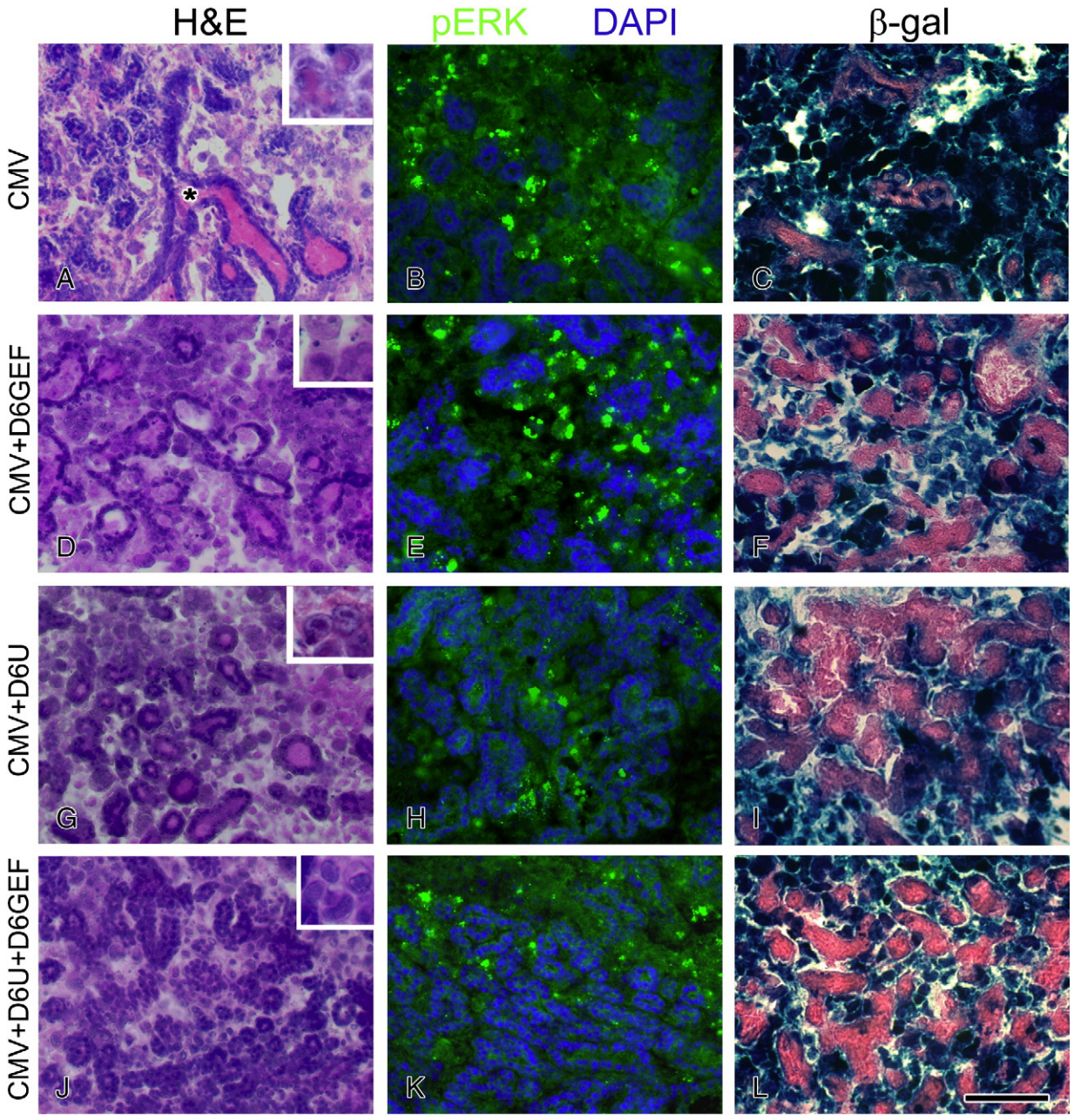

Fig. 2. Effect of EGFR→ERK inhibitors on histopathology, pERK expression and viral distribution in mCMV-infected NB + 14 SMGs. A–C. Untreated mCMV-infected SMGs (A) exhibit significant viral CPE, dilated lumina (*) and increased pERK immunolocalization (B). β-Galactosidase-stained virus (C) is densely distributed throughout abnormal stroma, and to a lesser extent, in abnormal epithelia. D–F. GEF-treated, mCMV-infected SMGs. In mCMV-infected SMGs treated with GEF beginning on day 6 (CMV + D6GEF), there is a small phenotypic improvement (compare D to AD), with pERK immunolocalization being similar to that seen in untreated SMGs (compare E to B). However, there is a slight decrease in β-galactosidase staining compared to untreated SMGs; there is an increase in eosin-stained pink (compare F to C). G–I. mCMV-infected SMGs treated with U0126 beginning on day 6 (CMV + D6U). In U0126-treated SMGs (G), a greatly improved phenotype is seen compared to untreated SMGs, with increased epithelial branching, reduced ductal dilation and a decrease in immunodetectable pERK and β-galactosidase-stained virus being seen (compare G to A, H to B and I to C). J-L. mCMV-infected SMGs treated with U0126 + GEF beginning on day 6. U0126 + GEF treatment results in an improved epithelial phenotype compared to untreated, GEF-treated, or U0126-treated mCMV-infected SMGs (compare J to A, D, G), with a marked increase in epithelial branching and absence of dilated lumina. Compared to untreated SMGs, a decrease in immunodetectable pERK (compare K to B) and β-galactosidase-stained virus (compare L to C) is seen. However, viral CPE (J) and β-galactosidase-stained virus (L) in the stroma persist. Insets A, D, G, J. High magnification showing viral CPE and pathognomonic kidney-shaped nuclei in stroma. Bar: A, D.G, J — 60 μm; B, C, E, F, K–L — 50 μm; insets 30 μm.

(Melnick et al., 2006, 2011). Here we investigated the question of whether mCMV replication is necessary for progressive pathogenesis with or without the presence of the EGFR→ERK pathway inhibitors. To answer this question, we utilized acyclovir, an antiherpesviral nucleoside active against mCMV (Burns et al., 1981).

NB SMGs were infected with 1×10^5 PFU/ml mCMV for 24 h and then cultured in control medium to day 6, allowing for several viral replication cycles; NB + 6 SMGs were then cultured in control medium with or without 10 μg/ml acyclovir, with or without EGFR→ERK pathway inhibitor, U0126 (or GEF, not shown), for an additional 8 days (a total of 14 days in culture). At NB + 14, explants treated with acyclovir show evident inhibition of mCMV replication (compare Fig. 5I to F); concomitantly, the SMGs are histologically nearing normal with increased epithelial branching, fewer dilations, and greatly reduced abnormal stroma (compare Fig. 5G to A); pERK expression is similar to that seen in controls and markedly less than in untreated mCMV-infected SMGs

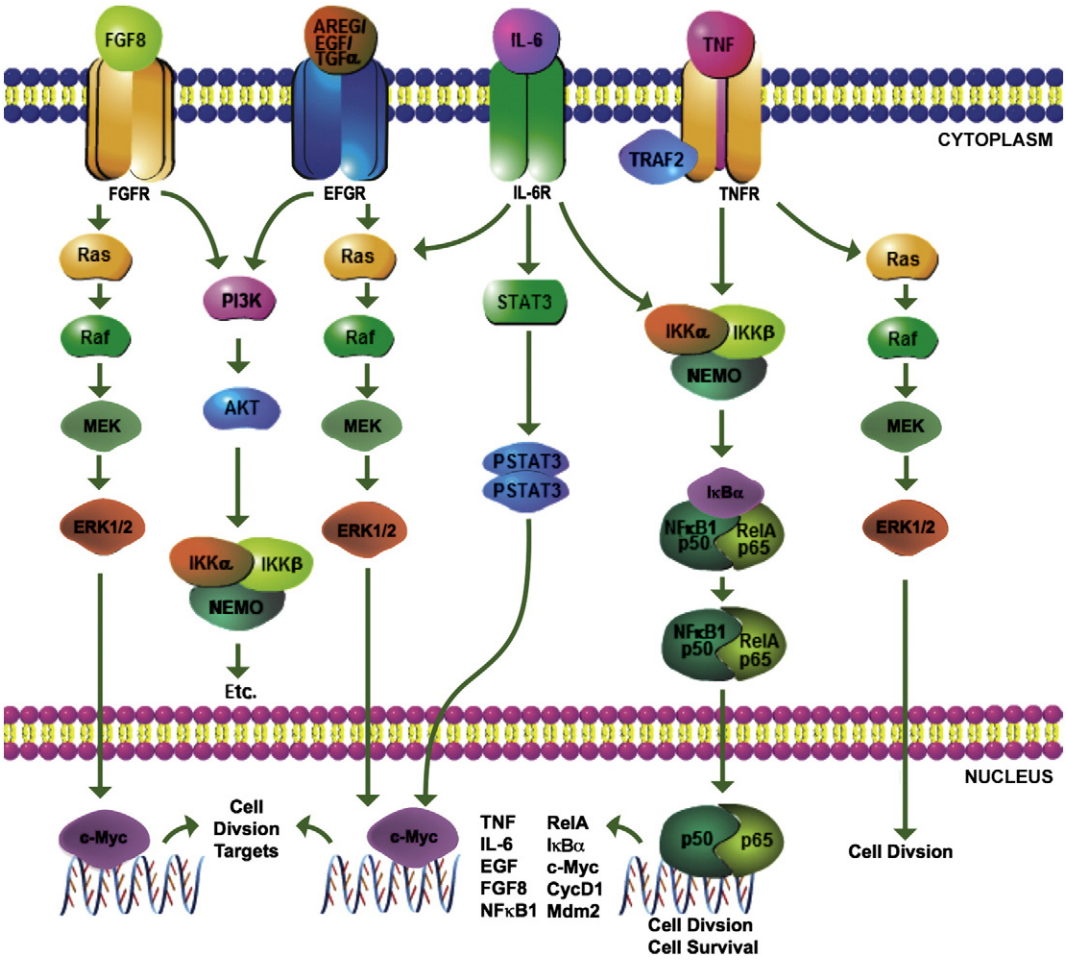

Fig. 3. Subcircuit map: a relational model that postulates how signaling events likely propagate during SMG pathogenesis; a conceptionally simple subcircuit for subsequent network modeling that is experimentally constrained and computationally accessible. This subcircuit is composed of 4 signaling pathways that are known to be critical to SMG ontogeny and share post-activation downstream targets (see text).

Table 1
mCMV Modulation of NB + 6 SMG ERK pathway ligand gene expression.

Gene	Control			mCMV			mCMV v. Control
	R	η	p	R	η	p	p
Areg	10.59	0.54	0.01	37.99	0.40	0.01	0.01
Egf	0.04	0.53	0.001	0.03	0.79	0.001	ns
Tgf-α	0.75	0.22	0.02	0.52	0.08	0.001	0.01
Fgf8	0.44	0.20	0.001	2.35	0.39	0.02	0.001
Il-6	10.50	0.71	0.05	679.83	0.54	0.01	0.001
Tnf-α	5.42	0.15	0.001	10.27	0.28	0.001	0.01

R = mean relative expression ratio (NB + 6/NB + 0) for control (uninfected) and mCMV-infected SMG explants.
η = gene expression noise = s_R/R (where s_R = standard deviation of R).
p = α probability level ("significance"); ns = not significant (p > 0.05).

(compare Fig. 5H to B, E). NB + 6 mCMV-infected SMGs concurrently treated with 10 μM U0126 and acyclovir for an additional 8 days (a total of 14 days in culture) show a normal SMG phenotype with considerable epithelial branching, a sparse fibromyxoid stroma, and no evidence of viral CPE (compare Fig. 5J to A) or viral presence (compare Fig. 5L to C, F). pERK expression is similar to that seen in controls (compare Fig. 5K to B). This completely rescued phenotype markedly differs from that seen with U0126 treatment alone (compare Figs. 5J–L to 2G–I); the U0126-treated, mCMV-infected SMGs exhibit some phenotypic improvement compared to untreated, mCMV-infected SMGs (compare Fig. 2G to A, 5D), but are still characterized by abnormal stroma and epithelia (compare Fig. 2G to 5J), increased pERK immunostaining (compare Fig. 2H to 5K) and considerable mCMV expression (compare Fig. 2I to 5L). These results indicate that persistent mCMV replication is necessary to maintain the viral cytopathic effect. Additionally, the need to further inhibit ERK phosphorylation (Figs. 5J–L) suggests that, even in the near absence of viral replication (Figs. 5I, L), there remains sufficient cellular memory (see Jullien and Gurdon, 2005) to preclude total elimination of stromal pathology (compare Fig. 5G to J) by day 14 in culture.

Discussion

Mucoepidermoid carcinoma (MEC) is the most common malignant tumor originating in major and minor salivary glands, accounting for almost one-third of all SG carcinomas (Lujan et al., 2010;

Fig. 4. mCMV induced AREG, FGF8, IL-6 and TNF-α protein immunodetection. A–H. Immunolocalization of AREG (A–B), FGF8 (C–D), IL-6 (E–F) and TNF-α (G–H) in control and mCMV-infected NB + 14 SMGs. With mCMV infection, there a notable increase in immunodetectable AREG, FGF8, IL-6, and TNF-α in abnormal stroma compared to controls (compare B to A, D to C, F to E, H to G). Bar: 40 μm I. Probabalistic neural network analysis was used to determine the contribution of *Areg*, *Fgf8*, *Il-6* and *Tnf-α* to the unbiased classification of SMG organs as either mCMV-infected or uninfected (control) with 100% sensitivity and 100% specificity. *Fgf8* and Il6 are of greater importance than *Areg* or *Tnfα*.

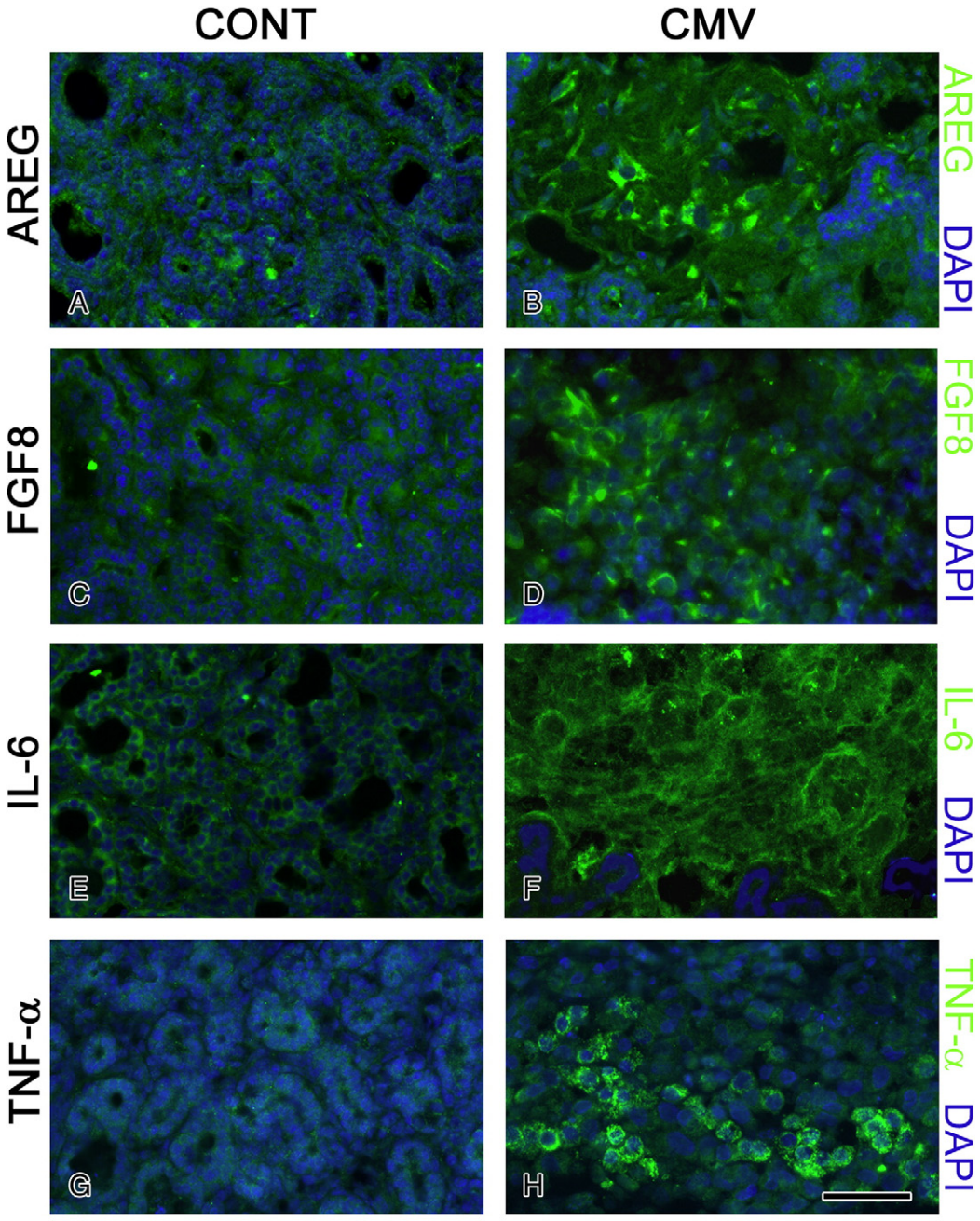
CONT
CMV
AREG
FGF8
IL-6
TNF-α
AREG DAPI
FGF8 DAPI
IL-6 DAPI
TNF-α DAPI
A
B
C
D
E
F
G
H

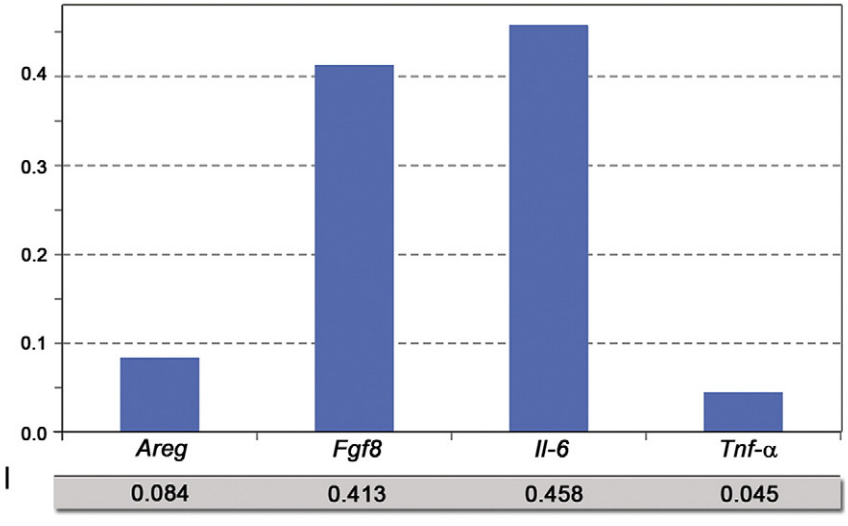
0.4
0.3
0.2
0.1
0.0
Areg
Fgf8
Il-6
Tnf-α
I
0.084
0.413
0.458
0.045

Schwarz et al., 2011). Although the precise etiology of MEC is largely unknown, we have recently shown that cytomegalovirus is an important component of MEC tumorigenesis (Melnick et al., 2011, 2012). Despite the well-documented overexpression of the EGFR→ERK signaling pathway in MEC (Akrish et al., 2009; Ito et al., 2009; Lujan et al., 2010), there has been limited to no success with inhibition of this pathway (Bell and Hanna, 2012; Gillespie et al., 2012), not unlike that seen with other malignancies (Engelman and Settleman, 2008). Using our previously described mouse model of CMV-induced SG dysplasia/neoplasia (Jaskoll et al., 2011; Melnick et al., 2011), we provide evidence that concurrent inhibition of ERK phosphorylation and inhibition of CMV replication obviates progressive pathogenesis and results in complete SG rescue (regression). These findings provide a mechanistic foundation for clinical trials that utilize similar concurrent treatment with extant FDA-approved drugs.

CMV has evolved numerous strategies to co-opt and alter host cell signaling networks for the purpose of propagating ever more virus (Sanchez and Spector, 2008; Schleiss, 2011). Cells respond to environmental challenges such as viral infection by reconfiguring regulated gene expression either by slow transcriptional adaptation or rapid post-transcriptional adaptation (Chalancon et al., 2012). The gene expression programs of signaling networks maintain homeostatic function at any given moment in a cell's life cycle. Corruption of these programs by a virus such as CMV can result in the host cell and tissue chaos we call dysplasia, neoplasia, and metaplasia.

Given the considerable crosstalk and redundancy in mammalian host cells, and the multifunctional paths mediated by single molecular components, a deep understanding of the subversion and dysregulation of the SMG interactome by CMV is a priori quite daunting (Gulbahce et al., 2012). For example, all the distinct ways in which mere 10 heterogeneous proteins can interact can be calculated as Bell's number (B_n), which in this case is 1.16×10^5 (Koch, 2012). Even if we assume that only 1 per 1000 of these potential interactions are biologically relevant, the number to be characterized would be 116, a task likely to consume the lifetime of most laboratories. In reality, of course, we must consider far more proteins and their millions of potential interactions. A way to circumvent this bad news, is to study groups of proteins as interacting single pathway modules (e.g. Fig. 3); correspondingly, the number of potential interactions precipitously declines (Koch, 2012). In this way, systematic analysis of virus-corrupted host cell targets should more easily identify dysregulated host cell networks relevant to viral-implicated tumorigenesis (Rozenblatt-Rosen et al., 2012).

We had every reason to initially assume that either single or co-targeted small molecule inhibition of the EGFR→ERK pathway would result in the complete rescue of SMG pathology (Little et al., 2011; Melnick et al., 2011; Poulikakos and Solit, 2011; Sturm et al., 2010). This proved not to be the case (Fig. 2). To be sure, there was a preclusion of progressive pathogenesis (stability, if you will), even in the continued presence of active CMV. This phenomenon has recently been termed diseases tolerance, i.e. the reduction of the negative impact of an infection on host fitness without directly affecting the pathogen (Medzhitov et al., 2012). Here, specifically, small molecule inhibitors "protected" the SMGs from further destructive pathogenesis independently of CMV load (Fig. 2). All this notwithstanding, failure to rescue SMG pathology suggested to us that other mediators whose signals converge downstream on the ERK pathway remain functional; even in the presence of the highest nontoxic dose of U0126 (an inhibitor of MEK-mediated ERK phosphorylation), pERK protein was undiminished (Fig. 2).

Recently, Wilson et al. (2012) presented convincing evidence that resistance to inhibitors of "oncogenic" kinase (e.g. gefitinib) results from an increase in the ligand levels of alternative pathways that share cell proliferation and survival effectors (ERK and PI3K), i.e. they share similar signaling outputs. Here we present data which supports this proposition. Namely, there is a highly significant upregulation of ligands for the FGFR, IL-6R and TNFR signaling pathways (Table 1; Fig. 4), all of which converge upon the Raf/MEK/ERK amplifier module (Fig. 3). These findings are clearly expositive of the failed attempt to simply inhibit EGFR-initiated, MEK mediated, ERK phosphorylation and effect complete rescue of the SMG explants (Fig. 2). It is interesting to note that all relevant ligands (AREG, FGF8, IL-6, TNF-α) are immunolocalized to the abnormal stroma of the CMV-infected SMGs, as is downstream pERK (Figs. 1, 4). This highlights the importance of the stromal microenvironment to progressive pathogenesis, regardless of the degree to which stromal paracrine stimulation participates in the epithelial pathogenesis (Hanahan and Weinberg, 2011; Pietras and Ostman, 2010). Indeed, FGF and IL-6 are both highly expressed by tumor-associated fibroblasts in a variety of tumor types (Bhowmick et al., 2004), and here they are relatively most important in characterizing the mCMV-induced pathologic phenotype (Fig. 4I).

hCMV-mediated overexpression of IL-6 and TNF-α has previously been reported (Zheng et al., 2012). Further, overexpression of the EGFR, FGFR, IL-6R, and TNFR pathways have been seen in human SG-MEC and other solid tumors (Azevedo et al., 2011; Elo et al., 2010; Ettl et al., 2012; Leivo et al., 2005; Mocellin et al., 2005). All of these pathways modulate cell proliferation and cell survival. Untoward upregulation of these particular multifunctional pathways mimics what we and others have shown in normal SG organogenesis (Jaskoll and Melnick, 1999; Jaskoll et al., 2002, 2004; Kashimata et al., 2000; Koyama et al., 2003; Melnick and Jaskoll, 2000; Melnick et al., 2001a,b,c). Drawing on the evermore apparent parallels between organogenesis and tumorigenesis (e.g. Becker et al., 2012), it should be noted that the EGFR, FGFR, IL-6R and TNFR pathways are not likely to be functionally independent (Jaskoll et al., 2002, 2004; Melnick et al., 2001a,c), but rather part of a larger network whose operational hub is NFκB (Melnick and Jaskoll, 2000; Melnick et al., 2001b; Fig. 3). This has been proffered for human tumors as well (Karin et al., 2002). Thus, it is becoming increasingly apparent that shared embryonic and tumor genetic signatures may be prognostically important (Becker et al., 2012).

Conclusion

CMV is a principle element in the multifactorial causation of human salivary gland mucoepidermoid carcinoma. Despite the well-documented overexpression of the EGFR→ERK signaling pathway in SG-MEC, there has been little clinical success with inhibition strategies. It has been proposed that failed inhibition results from an increase in the ligand levels of alternative pathways that share cell proliferation and survival effectors (ERK, PI3K). In support of this proposition, we present mouse model evidence of a highly significant upregulation of ligands for the FGFR, IL-6R and TNFR signaling pathways, all of which converge upon the Raf/MEK/ERK amplifier module. These finding are clearly expositive of the failed attempt to simply inhibit EGFR-initiated, MEK-mediated, ERK phosphorylation and effect complete rescue. Here we model a potential solution that obviates progressive pathogenesis and effects complete SG rescue (regression), namely the concurrent inhibition of ERK phosphorylation (U0126) and CMV replication (acyclovir).

Conflict of interests

The authors declare that there are no conflicts of interest.

List of abbreviations

AREG	amphiregulin
CMV	cytomegalovirus
CONT	control
CRTC1	CREB-regulated transcription coactivator 1
DAPI-4′,6	Diamidino-2-phenylindole, dihydrochloride

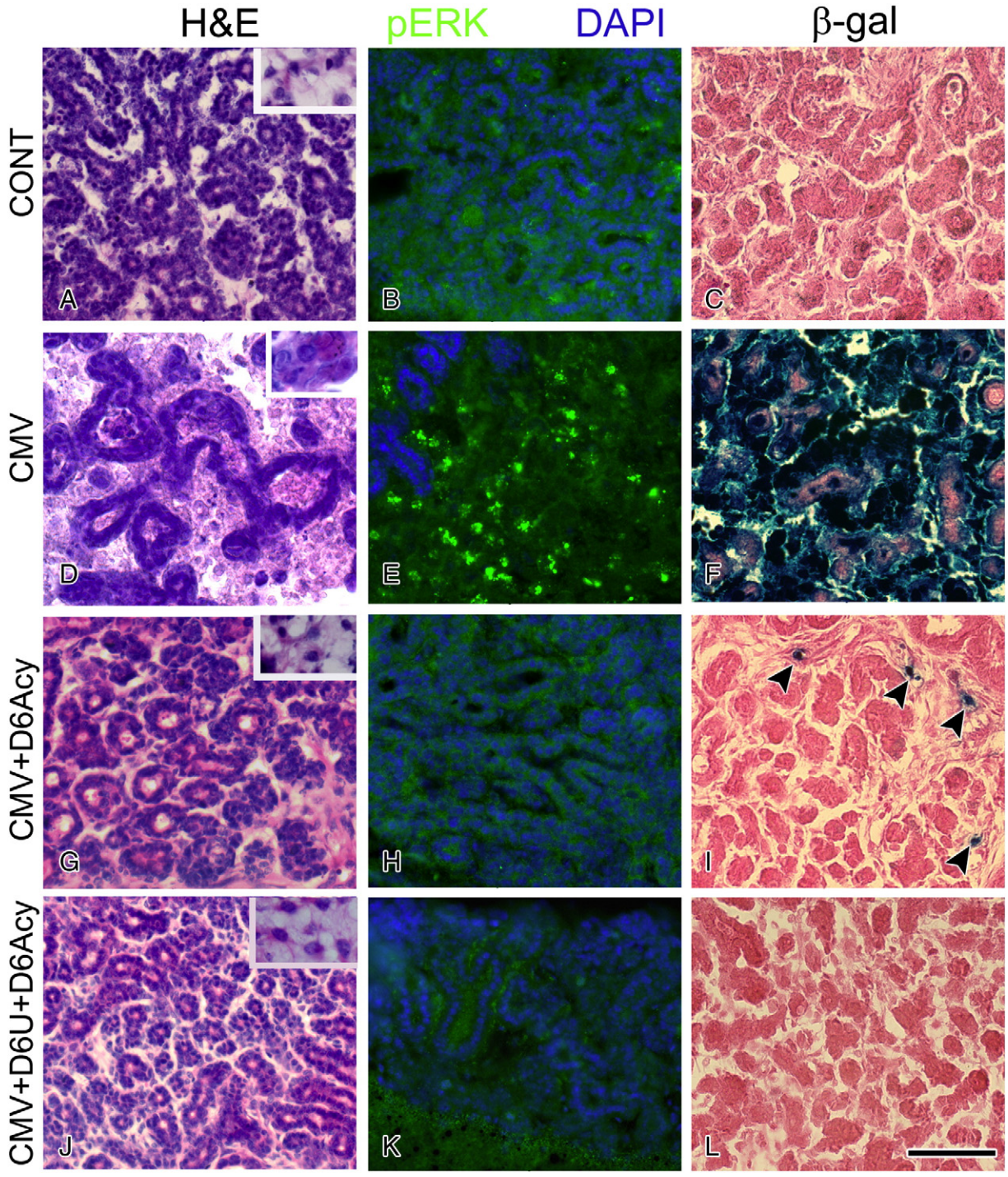

Fig. 5. mCMV-replication is essential for progressive pathogenesis and pERK expression in NB + 14 SMGs. A–C. Control SMGs. Control SMGs exhibit a normal ductal and acinar epithelia embedded in a fibromyxoid stroma consisting of stellate to ovoid fibroblasts. A, inset. High magnification of stellate fibroblasts. Note the absence of immunodetectable pERK (B) and β-galactosidase staining (C) in controls. D-F. mCMV-infected SMGs. With mCMV infection, abnormal epithelia and stroma, as well as increased immunodetectable pERK (compare E to B), are seen; β-galactosidase-stained virus is seen throughout abnormal stroma and, to a lesser extent, in epithelia (compare F to C). D, inset. High magnification of viral CPE in stroma. G-I. mCMV-infected SMGs treated with acyclovir beginning on day 6 (CMV + D6Acy). With acyclovir-treatment, there is a marked improvement in epithelial and stromal morphology compared to untreated, mCMV-infected SMGs (compare G to D) and little β-galactosidase-stained virus (arrowheads) (I). However, ductal and acini exhibit a pseudo-stratified, hyperplastic epithelium surrounding lumina rather than the cuboidal epithelium seen in controls (compare G to A). pERK immunolocalization is similar to that seen in controls (compare H to B) and markedly less than in mCMV-infected SMGs (compare H to E). G inset. High magnification of stroma showing normal stellate fibroblasts and the absence of viral CPE. J–L. mCMV-infected SMGs treated with U0126 + acyclovir beginning on day 6 (CMV + D6U + D6 ACY). The addition of U0126 to acyclovir-treated SMGs results in normal epithelial and stromal morphology (compare J to A, D), the absence of β-galactosidase-stained virus (compare L to C), and pERK immunolocalization resembling control (compare K to B). J inset. High magnification showing normal stellate fibroblast and absence of viral CPE in stroma. Bar: A, C, D, F, G, I, J, L — 60 μm; B, E, H, K — 50 μm; insets — 30 μm.

ERK	extracellular signal-regulated protein kinases 1 and 2 (ERK1/2
EGFR	epidermal growth factor receptor
GEF	gefitinib
hCMV	human cytomegalovirus
mCMV	mouse cytomegalovirus
MEK	mitogenactivated protein kinase kinase
NB	newborn
NFA	negative feedback amplifier
pERK	phosphorylated ERK1/2
PFU	plaque forming units
PNN	Probabilistic neural network analysis
qRT-PCR	quantitative RT-PCR
Raf	rapidly accelerated fibrosarcoma oncogene
Ras	rat sarcoma viral oncogene
RTK	receptor tyrosine kinase
SG	salivary gland
SMG	salivary gland
SOS	guanine nucleotide exchange factors son of sevenless oncogene
TK	tyrosine kinase

Acknowledgments

We would like to thank Dr. Edward Mocarski for his generous gift of mCMV. This research was supported by the Oral Biology Fund of the University of Southern California.

References

Akrish, S., Peled, M., Ben-Izhak, B., Nagler, R.M., 2009. Malignant salivary gland tumors and cyclo-oxygenase-2: a histopathological and immunohistochemical analysis with implications on histogenesis. Oral Oncology 45, 1044–1050.

Alwine, J.C., 2012. The human cytomegalovirus assembly compartment: a masterpiece of viral manipulation of cellular processes that facilitates assembly and egress. PLoS Pathogens 8, e1002878.

Azevedo, A., Cunha, V., Teixeira, A.L., Medeiros, R., 2011. IL-6/IL-6R as a potential key signaling pathway in prostate cancer development. World Journal of Clinical Oncology 2, 384–396.

Becker, D., Sfakianakis, I., Krupp, M., Staib, F., Gerhold-Ay, A., Victor, A., Binder, H., Blettner, M., Maass, T., Thorgeirsson, S., Galle, P.R., Teufel, A., 2012. Genetic signatures shared in embryonic liver development and liver cancer define prognostically relevant subgroups in HCC. Molecular Cancer 11, 55.

Bell, D., Hanna, E.Y., 2012. Salivary gland cancers: biology and molecular targets for therapy. Current Oncology Reports 14, 166–174.

Bhowmick, N.A., Neilson, E.G., Moses, H.L., 2004. Stromal fibroblasts in cancer initiation and progression. Nature 432, 332–337.

Boppana, S.B., Fowler, K.B., 2007. Persistence in the Population: Epidemiology and Transmission. Cambridge University Press, Cambridge, Mass.

Burns, W.H., Wingard, J.R., Bender, W.J., Saral, R., 1981. Thymidine kinase not required for antiviral activity of acyclovir against mouse cytomegalovirus. Journal of Virology 39, 889–893.

Chalancon, G., Kruse, K., Babu, M.M., 2012. Cell biology. Reconfiguring regulation. Science 335, 1050–1051.

Chen, C. (Ed.), 1996. Fuzzy Logic and Neural Network Handbook. McGraw-Hill, New York.

Elo, T.D., Valve, E.M., Seppänen, J.A., Vuorikoski, H.J., Mäkelä, S.I., Poutanen, M., Kujala, P.M., Härkönen, P.L., 2010. Stromal activation associated with development of prostate cancer in prostate-targeted fibroblast growth factor 8b transgenic mice. Neoplasia 12, 915–927.

Engelman, J.A., Settleman, J., 2008. Acquired resistance to tyrosine kinase inhibitors during cancer therapy. Current Opinion in Genetics and Development 18, 73–79.

Ettl, T., Stiegler, C., Zeitler, K., Agaimy, A., Zenk, J., Reichert, T.E., Gosau, M., Kühnel, T., Brockhoff, G., Schwarz, S., 2012. EGFR, HER2, survivin, and loss of pSTAT3 characterize high-grade malignancy in salivary gland cancer with impact on prognosis. Human Pathology 43, 921–931.

Gillespie, M.B., Albergotti, W.G., Eisele, D.W., 2012. Recurrent salivary gland cancer. Current Treatment Options in Oncology 13, 58–70.

Goldberg, D.E., 1989. Genetics Algorithms in Search, Optimization, and Machine Learning. Addison-Wesley, Reading, Mass.

Gulbahce, N., Yan, H., Dricot, A., Padi, M., Byrdsong, D., Franchi, R., Lee, D.S., Rozenblatt-Rosen, O., Mar, J.C., Calderwood, M.A., Baldwin, A., Zhao, B., Santhanam, B., Braun, P., Simonis, N., Huh, K.W., Hellner, K., Grace, M., Chen, A., Rubio, R., Marto, J.A., Christakis, N.A., Kieff, E., Roth, F.P., Roecklein-Canfield, J., Decaprio, J.A., Cusick, M.E., Quackenbush, J., Hill, D.E., Münger, K., Vidal, M., Barabási, A.L., 2012. Viral perturbations of host networks reflect disease etiology. PLoS Computational Biology 8, e1002531.

Hanahan, D., Weinberg, R.A., 2011. Hallmarks of cancer: the next generation. Cell 144, 646–674.

Ito, F.A., Coletta, R.D., Graner, E., de Almeida, O.P., Lopes, M.A., 2009. Salivary gland tumors: immunohistochemical study of EGF, EGFR, ERbB-2, FAS and Ki-67. Analytical and Quantitative Cytology and Histology 31, 280–287.

Jaskoll, T., Melnick, M., 1999. Submandibular gland morphogenesis: stage-specific expression of TGF-alpha/EGF, IGF, TGF-beta, TNF, and IL-6 signal transduction in normal embryonic mice and the phenotypic effects of TGF-beta2, TGF-beta3, and EGF-r null mutations. Anatomical Record 256, 252–268.

Jaskoll, T., Zhou, Y.M., Chai, Y., Makarenkova, H.P., Collinson, J.M., West, J.D., Hajihosseini, M.K., Lee, J., Melnick, M., 2002. Embryonic submandibular gland morphogenesis: stage-specific protein localization of FGFs, BMPs, Pax6 and Pax9 in normal mice and abnormal SMG phenotypes in FgfR2-IIIc(+/Delta), BMP7(-/-) and Pax6(-/-) mice. Cells, Tissues, Organs 170, 83–98.

Jaskoll, T., Witcher, D., Toreno, L., Bringas, P., Moon, A.M., Melnick, M., 2004. FGF8 dose-dependent regulation of embryonic submandibular salivary gland morphogenesis. Developmental Biology 268, 457–469.

Jaskoll, T., Htet, K., Abichaker, G., Kaye, F.J., Melnick, M., 2011. CRTC1 expression during normal and abnormal salivary gland development supports a precursor cell origin for mucoepidermoid cancer. Gene Expression Patterns 11, 57–63.

Jullien, J., Gurdon, J., 2005. Morphogen gradient interpretation by a regulated trafficking step during ligand-receptor transduction. Genes & Development 19, 2682–2694.

Karin, M., C. Y., Greten, F.R., Li, Z.W., 2002. NF-kappaB in cancer: from innocent bystander to major culprit. Nature Reviews. Cancer 2, 301–310.

Kashimata, M., Sayeed, S., Ka, A., Onetti-Muda, A., Sakagami, H., Faraggiana, T., Gresik, E.W., 2000. The ERK-1/2 signaling pathway is involved in the stimulation of branching morphogenesis of fetal mouse submandibular glands by EGF. Developmental Biology 220, 183–196.

Koch, C., 2012. Systems biology. Modular biological complexity. Science 337, 531–532.

Koyama, N., Kashimata, M., Sakashita, H., Sakagami, H., Gresik, E.W., 2003. EGF-stimulated signaling by means of PI3K, PLCgamma1, and PKC isozymes regulates branching morphogenesis of the fetal mouse submandibular gland. Developmental Dynamics 227, 216–226.

Leivo, I., Jee, K.J., Heikinheimo, K., Laine, M., Ollila, J., Nagy, B., Knuutila, S., 2005. Characterization of gene expression in major types of salivary gland carcinomas with epithelial differentiation. Cancer Genetics and Cytogenetics 156, 104–113.

Little, A.S., Balmanno, K., Sale, M.J., Newman, S., Dry, J.R., Hampson, M., Edwards, P.A., Smith, P.D., Cook, S.J., 2011. Amplification of the driving oncogene, KRAS or BRAF, underpins acquired resistance to MEK1/2 inhibitors in colorectal cancer cells. Science Signaling 4, ra17.

Lujan, B., Hakim, S., Moyano, S., Nadal, A., Caballero, M., Diaz, A., Valera, A., Carrera, M., Cardesa, A., Alos, L., 2010. Activation of the EGFR/ERK pathway in high-grade mucoepidermoid carcinomas of the salivary glands. British Journal of Cancer 103, 510–516.

Medzhitov, R., Schneider, D.S., Soares, M.P., 2012. Disease tolerance as a defense strategy. Science 335, 936–941.

Melnick, M., Jaskoll, T., 2000. Mouse submandibular gland morphogenesis: a paradigm for embryonic signal processing. Critical Reviews in Oral Biology and Medicine 11, 199–215.

Melnick, M., Chen, H., Zhou, Y.M., Jaskoll, T., 2001a. Interleukin-6 signaling and embryonic mouse submandibular salivary gland morphogenesis. Cells, Tissues, Organs 168, 233–245.

Melnick, M., Chen, H., Min Zhou, Y., Jaskoll, T., 2001b. The functional genomic response of developing embryonic submandibular glands to NF-kappa B inhibition. BMC Developmental Biology 1, 15.

Melnick, M., Chen, H., Zhou, Y., Jaskoll, T., 2001c. Embryonic mouse submandibular salivary gland morphogenesis and the TNF/TNF-R1 signal transduction pathway. Anatomical Record 262, 318–330.

Melnick, M., Mocarski, E.S., Abichaker, G., Huang, J., Jaskoll, T., 2006. Cytomegalovirus-induced embryopathology: mouse submandibular salivary gland epithelial–mesenchymal ontogeny as a model. BMC Developmental Biology 6, 42.

Melnick, M., Phair, R.D., Lapidot, S.A., Jaskoll, T., 2009. Salivary gland branching morphogenesis: a quantitative systems analysis of the Eda/Edar/NFkappaB paradigm. BMC Developmental Biology 9, 32.

Melnick, M., Abichaker, G., Htet, K., Sedghizadeh, P., Jaskoll, T., 2011. Small molecule inhibitors of the host cell COX/AREG/EGFR/ERK pathway attenuate cytomegalovirus-induced pathogenesis. Experimental and Molecular Pathology 1, 400–410.

Melnick, M., Sedghizadeh, P.P., Allen, C.M., Jaskoll, T., 2012. Human cytomegalovirus and mucoepidermoid carcinoma of salivary glands: cell-specific localization of active viral and oncogenic signaling proteins is confirmatory of a causal relationship. Experimental and Molecular Pathology 92, 118–125.

Mocellin, S., Rossi, C.R., Pilati, P., Nitti, D., 2005. Tumor necrosis factor, cancer and anticancer therapy. Cytokine & Growth Factor Reviews 16, 35–53.

Nichols, W.G., Boeckh, M., 2000. Recent advances in the therapy and prevention of CMV infections. Journal of Clinical Virology 16, 25–40.

Pietras, K., Ostman, A., 2010. Hallmarks of cancer: interactions with the tumor stroma. Experimental Cell Research 316, 1324–1331.

Poulikakos, P.I., Solit, D.B., 2011. Resistance to MEK inhibitors: should we co-target upstream? Science Signaling 4, pe16.

Raser, J.M., O'Shea, E.K., 2005. Noise in gene expression: origins, consequences, and control. Science 309, 2010–2013.

Rozenblatt-Rosen, O., Deo, R.C., Padi, M., Adelmant, G., Calderwood, M.A., Rolland, T., Grace, M., Dricot, A., Askenazi, M., Tavares, M., Pevzner, S.J., Abderazzaq, F., Byrdsong, D., Carvunis, A.R., Chen, A.A., Cheng, J., Correll, M., Duarte, M., Fan, C., et al., 2012. Interpreting cancer genomes using systematic host network perturbations by tumour virus proteins. Nature 487, 491–495.

Saederup, N., Lin, Y.C., Dairaghi, D.J., Schall, T.J., Mocarski, E.S., 1999. Cytomegalovirus-encoded beta chemokine promotes monocyte-associated viremia in the host.

Proceedings of the National Academy of Sciences of the United States of America 96, 10881–10886.
Sanchez, V., Spector, D.H., 2008. Subversion of cell cycle regulatory pathways. Current Topics in Microbiology and Immunology 325, 243–262.
Schleiss, M.R., 2011. Congenital cytomegalovirus infection: molecular mechanisms mediating viral pathogenesis. Infectious Disorders Drug Targets 11, 449–465.
Schwarz, S., Stiegler, C., Müller, M., Ettl, T., Brockhoff, G., Zenk, J., Agaimy, A., 2011. Salivary gland mucoepidermoid carcinoma is a clinically, morphologically and genetically heterogeneous entity: a clinicopathological study of 40 cases with emphasis on grading, histological variants and presence of the t(11;19) translocation. Histopathology 58, 557–570.
Specht, D., 1988. Probabilistic neural network for classification, mapping, or associative memory. Proceeding of the IEEE International Conference on Neural Networks, 1, pp. 525–532.
Specht, D., Shapiro, P., 1991. Generalization accuracy of probabilistic neural networks captured with back-propagation networks. Proceeding of the IEEE International Joint Conference on Neural Networks, 1, pp. 887–892.
Sturm, O.E., Orton, R., Grindlay, J., Birtwistle, M., Vyshemirsky, V., Gilbert, D., Calder, M., Pitt, A., Kholodenko, B., Kolch, W., 2010. The mammalian MAPK/ERK pathway exhibits properties of a negative feedback amplifier. Science Signaling 3, ra90.
Tirado, Y., Williams, M.D., Hanna, E.Y., Kaye, F.J., Batsakis, J.G., El-Naggar, A.K., 2007. CRTC1/MAML2 fusion transcript in high grade mucoepidermoid carcinomas of salivary and thyroid glands and Warthin's tumors: implications for histogenesis and biologic behavior. Genes, Chromosomes & Cancer 46, 708–715.
Wagner, R.P., Tian, H., McPherson, M.J., Latham, P.S., Orenstein, J.M., 1996. AIDS-associated infections in salivary gland: autopsy survey of 60 cases. Clinical Infectious Diseases 22, 369–371.
Wilson, T.R., Fridlyand, J., Yan, Y., Penuel, E., Burton, L., Chan, E., Peng, J., Lin, E., Wang, Y., Sosman, J., Ribas, A., Li, J., Moffat, J., Sutherlin, D.P., Koeppen, H., Merchant, M., Neve, R., Settleman, J., 2012. Widespread potential for growth-factor-driven resistance to anticancer kinase inhibitors. Nature 487, 505–509.
Yuan, J., Liu, X., Wu, A., McGonagill, P., Keller, M., Galle, C., Meier, J., 2009. Breaking human cytomegalovirus major immediate-early gene silence by vasoactive intestinal peptide stimulation of the protein kinase A-CREB-TORC2 signaling cascade in human pluripotent embryonal NTera2 cells. Journal of Virology 83, 6391–6403.
Zheng, Q., Tao, R., Gao, H., Xu, J., Shang, S., Zhao, N., 2012. HCMV-encoded UL128 enhances TNF-α and IL-6 expression and promotes PBMC proliferation through the MAPK/ERK pathway in vitro. Viral Immunology 25, 98–105.